



Article

Magnesium Oxide and Magnesium Fluoride Nanopowders Produced in a Diffuse Nanosecond Discharge in Argon

Dmitry Beloplotov ^{1,*}, Konstantin Savkin ¹, Viktor Semin ² and Dmitry Sorokin ¹

¹ Institute of High Current Electronics SB RAS, 2/3, Akademicheskii Ave., 634055 Tomsk, Russia; savkinkp@mail2000.ru (K.S.); sdma-70@loi.hcei.tsc.ru (D.S.)

² Institute of Strength Physics and Materials Science SB RAS, 2/4, Akademicheskii Ave., 634055 Tomsk, Russia; viktor.semin.tsk@gmail.com

* Correspondence: rff.qep.bdim@gmail.com

Abstract: The synthesis of the nanopowders of magnesium oxide and magnesium fluoride during the operation of a repetitive diffuse nanosecond discharge in argon at various pressures was performed. Nanosecond voltage pulses with an amplitude of -70 kV, a rise time of 0.7 ns, and a duration of 0.7 ns were applied across a point-to-plane gap of 2 mm in length. The pulse repetition rate was 60 Hz. The high-voltage pointed electrode was made of magnesium. A diffuse discharge cold plasma was formed under these conditions. Nanoparticles were produced as a result of an explosion of microprotrusions on the surface of the magnesium electrode due to a high current density. Lines of magnesium atoms and ions were observed in the emission optical spectrum. Under the actions of the gas dynamics processes caused by the plasma channel expansion during the interpulse period, nanoparticles were deposited onto the surface of the grounded plane electrode and the side wall of the gas discharge chamber. The morphology, elemental, and phase composition of the powders were studied using transmission electron microscopy (TEM) and energy-dispersive X-ray spectroscopy (EDS).

Keywords: magnesium; magnesium oxide; magnesium fluoride; nanopowder; ceramics; diffuse nanosecond discharge; low-temperature plasma; atmospheric pressure plasma; TEM; EDS



Citation: Beloplotov, D.; Savkin, K.; Semin, V.; Sorokin, D. Magnesium Oxide and Magnesium Fluoride Nanopowders Produced in a Diffuse Nanosecond Discharge in Argon. *Ceramics* **2023**, *6*, 1467–1477. <https://doi.org/10.3390/ceramics6030090>

Academic Editor: Jose M.F. Ferreira

Received: 26 May 2023

Revised: 28 June 2023

Accepted: 4 July 2023

Published: 6 July 2023



Copyright: © 2023 by the authors. Licensee MDPI, Basel, Switzerland. This article is an open access article distributed under the terms and conditions of the Creative Commons Attribution (CC BY) license (<https://creativecommons.org/licenses/by/4.0/>).

1. Introduction

Ceramics are promising materials for application in various industries, owing to their unique physical and chemical properties [1]. They are used as functional materials for electronic devices and biomedical implants [2–5]. The production of ceramics has evolved significantly over the years. Various methods have been developed to produce these materials [6]. One of the most common approaches is the synthesis of powders and ceramic-bearing materials through high-temperature or high-pressure treatments. The resulting material is then shaped and further processed to obtain the final product.

Advancements in materials science have led to the development of nanopowders, which have great potential in the production of ceramics [7,8]. Nanopowders have a particle size of less than 100 nanometers. They have a high surface area-to-volume ratio, which increases their reactivity. This means that the powders can be sintered at lower temperatures, resulting in energy and cost savings. This has opened up the way to the production of nanoceramics with unique properties such as mechanical strength, electrical conductivity, chemical activity, thermal stability, and corrosion resistance, etc. These newly developed ceramic materials demonstrate new opportunities for various applications in electronics, catalysis, energy production and storage, medicine, and so forth [9–12].

Nanopowders can be obtained using various methods: sol-gel synthesis, hydrothermal synthesis, ball milling, and gas discharge. However, there are challenges associated with their production. One major problem is the approval of fabrication routes in order to produce ceramic nanomaterials possessing the required characteristics (size, shape and purity) under low-energy cost conditions.

Nanosecond gas discharge is one of the promising methods for obtaining nanopowders [13]. This method involves the use of a high-voltage nanosecond pulse to generate highly reactive low-temperature plasma in a gas mixture. Energetic species are produced in such plasma. They react with a precursor material, such as an electrode material, and form nanoparticles. The advantage of this method is its ability to produce nanoparticles with a controlled size and shape and its scalability for large-scale production. However, the issue of cost is still debatable for this method. One of the ways to reduce this cost is the rejection of vacuum systems and the transition to nanosecond discharges of atmospheric pressure. One of the problems of obtaining low-temperature plasma at atmospheric gas pressure is the discharge constriction and the formation of a spark, which reduces the quality of these nanopowders. Therefore, the goal of our work was to obtain high-quality, magnesium-containing nanopowders in a diffuse nanosecond discharge in argon and reveal the experimental conditions preventing a constriction of the discharge and formation of a spark. Magnesium oxide ceramic has an excellent thermal stability and low thermal expansion, making it ideal for use in thermal barrier coatings and electrical insulators [14].

2. Experimental Setup and Measurement Techniques

A sketch of an experimental powder generator based on a diffuse nanosecond gas discharge is presented in Figure 1a. The setup consisted of a gas discharge chamber, coaxial transmission line, and generator of high-voltage nanosecond pulses. The gas discharge chamber with the transmission line was primarily developed by us to perform studies on nanosecond discharges and cold plasmas in various gases in a wide pressure range and electrode configuration, both with optical (spectral) methods and through accurate measurements of the electrical parameters [15]. Nevertheless, it can be adapted for obtaining nanoparticles and optimized directly for the task of synthesis.

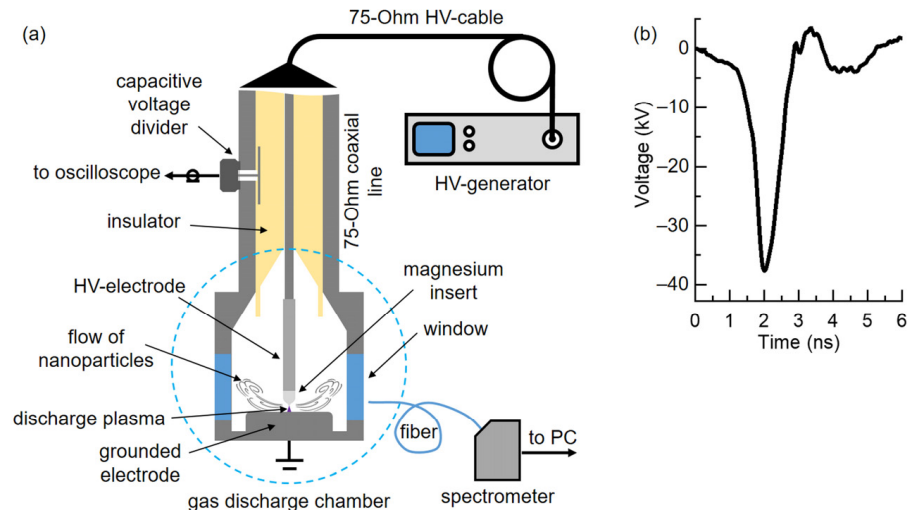


Figure 1. (a) Sketch of an experimental powder generator based on a nanosecond gas discharge. (b) Waveform of a voltage pulse at matched load (75 Ohm).

A nanosecond discharge was formed between the electrodes placed in a vacuum vessel. A high-voltage (HV) electrode was a metal tube 6 mm in diameter. A magnesium cone-shaped insert was installed at the end of the HV electrode. It should be noted that the magnesium alloy contained also aluminum (Al) up to 6.5 at. % and silicon (Si) up to 0.5 at. %. The grounded electrode was an aluminum disk with a rounded edge. The flat part of the grounded electrode faced the HV electrode. The distance between the electrodes was 2 mm. Such an electrode configuration provided an inhomogeneous distribution of the electric field.

Based on FID (fast ionization devices) technology [16], a GIN-55-01 generator produced nanosecond voltage pulses (Figure 1b), which were applied to the HV electrode via an

HV cable and the coaxial transmission line. The amplitude, rise time, full width at half maximum, repetition rate, pulse energy, and pulse power were ~ 38 kV (maximum), 0.7 ns, 0.7 ns, 50–60 Hz, 10 mJ, and 16 MW, respectively. It should be noted that the voltage pulse amplitude doubled when it arrived at the gap due to reflection (idling mode).

A capacitive voltage divider (CVD) was built into the transmission line of the discharge chamber. CVD was used to measure the voltage pulses propagating to the gap. The CVD-to-gap travel time was ≈ 0.5 ns. As a result, the CVD signal, U_{CVD} , presented a sum of the incident, U_{inc} , and reflected, U_{ref} , voltage pulses that were shifted in time relative to each other ≈ 1 ns. Nevertheless, since the waveform of U_{inc} was known (Figure 1b), the reflected pulse, U_{ref} , could be easily calculated from the U_{CVD} . The signals from the CVD, U_{CVD} , were recorded with an MSO64B (Tektronix, Inc., Beaverton, USA) oscilloscope (8 GHz, 20 GS/s). Knowing U_{inc} and U_{ref} , as well as the impedance, Z , of the transmission line, the current, I , could be calculated by $I = (U_{\text{inc}} - U_{\text{ref}})/Z$.

The gas discharge chamber was pumped out and then filled with argon (purity 99.999). The discharge operated at low (13 kPa) and elevated (110 kPa) pressures. The base pressure was 98–100 kPa. It turned out that 13 kPa was the pressure at which the discharge remained concentrated near the top of the cathode and did not develop in the side direction toward the chamber walls. At the same time, we wanted to study the effect of the pressure on the parameters of the powders. The elevated pressure prevented the penetration of outside air into the discharge chamber.

The windows of the discharge chamber were made of CaF_2 plates 5 mm thick and 40 mm in diameter. The transmission range of the plates was 0.13–10 μm . Emission spectra of the discharge plasma were taken with an HR2000 (Ocean Optics, Inc., Dunedin, FL, USA) spectrometer operating in the wavelength range of $\Delta\lambda = 190\text{--}1100$ nm. The spectral resolution of the spectrometer was ≈ 1.2 nm. The identification of the spectral lines of the atoms and ions was performed using the NIST database (National Institute of Standards and Technology, Gaithersburg, MD, USA) [17].

A EOS R full-frame (36 \times 24 mm) mirrorless 30.3 Megapixel camera (Canon, Inc., Ota, Tokyo, Japan) equipped with a K2 Distamax long-distance microscope (Infinity Photo-Optical Company, Centennial, CO, USA) with a CentriTel Focuser and CF-3 objective (optical resolution up to 1.7 μm) was used to take images of the discharge.

Nanoparticles, produced during the discharge, were deposited onto the surface of the grounded electrode and the side wall of the gas discharge chamber. After the depressurization of the chamber, the powder was scraped off and gathered into plastic containers for further structural characterization.

The structural parameters (shape, size, and phase composition) of the particles synthesized in the nanosecond discharge in argon were studied using a JEM 2100 transmission electron microscope (Jeol, Ltd., Akishima, Japan), operating at an accelerating voltage of 200 kV. The elemental composition was determined using an “INCA Energy” (Oxford Instruments, Abingdon, UK) energy-dispersive spectrometer (EDS) built-in transmission electron microscope. The quantitative analysis of the elemental composition was carried out by collecting the EDS spectra from individual particles (point analysis).

3. Results and Discussion

When applying the nanosecond voltage pulses across the gap, a diffuse discharge was formed at both pressures of argon (Figure 2). The extremely short rise time of the voltage pulse provided a high overvoltage of the gap. This means that a gas-filled discharge gap was broken down at voltages of an order of magnitude higher than the static breakdown voltage. For argon, the static breakdown voltage is 2.7 kV [18]. In our experiments, the breakdown voltage reached ≈ 76 kV.

The diffuse form of the nanosecond discharge at atmospheric pressure (Figure 2) was due to a high overvoltage, ensuring the development of a large-diameter streamer that crossed the gap and generated low-temperature non-equilibrium dense plasma [19] with a

high conductivity. The nanosecond duration prevented gas heating, which is the cause of the discharge constriction and spark formation.

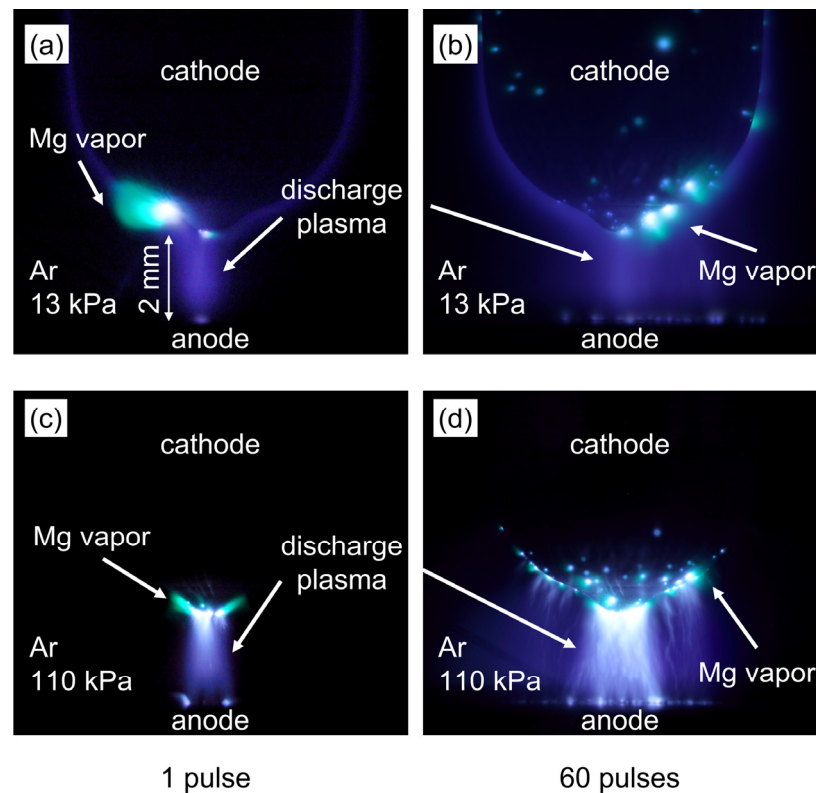


Figure 2. Images of the nanosecond discharge plasma in argon at a pressure of (a,b) 13 kPa, and (c,d) 110 kPa. Interelectrode distance is 2 mm.

Figure 3 shows the waveforms of the voltage pulses (U_{CVD} , U_{inc} , and U_{ref}) and corresponding current pulses calculated by $I = (U_{inc} - U_{ref})/Z$ during the discharge in argon at low (13 kPa) and elevated (110 kPa) pressures.

During the discharge, the current reached ≈ 400 A. It should be noted that the current was concentrated near the magnesium electrode tip with an area of $\sim 10^{-2}$ cm². Therefore, the current density reached $\sim 10^4$ A/cm². At such a high current density, the electroerosion of the electrode surface occurred. Microprotrusions on the tip surface exploded [20] and formed a dense metal plasma that expanded adiabatically. Due to the low temperature of the surrounding gas and discharge plasma, metal vapor condensed, resulting in the formation of nanoparticles [13]. However, at the plasma stage, metal atoms and ions could interact with gas atoms and ions, in particular with oxygen, forming metal oxides. The interaction between the metal atoms and ions and oxidant species could be of great interest in terms of material processing and the production of various compounds and nanoceramics.

The emission spectra of the nanosecond discharge plasma in argon at low and elevated pressures are presented in Figure 4.

The emission spectra are complex. The spectra are characterized by the presence of atomic or molecular transitions. First of all, argon lines (4p-4s transition) were observed in the wavelength range of 700–1000 nm. The wavelengths of the most intense lines are noted in Figure 4. It should also be noted that the spectral distance between some lines was shorter than the spectral resolution of the spectrometer (1.2 nm). Hence, two or more closely spaced lines look like one.

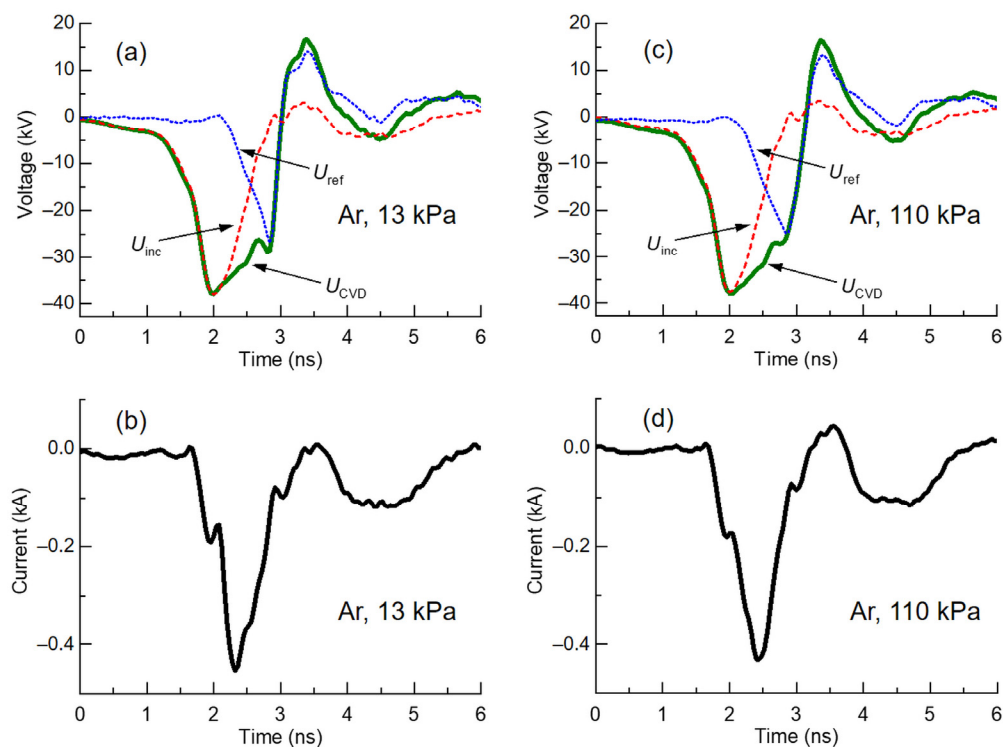


Figure 3. Waveforms of voltage and current during nanosecond discharge in argon at a pressure of (a,b) 13 kPa, and (c,d) 110 kPa.

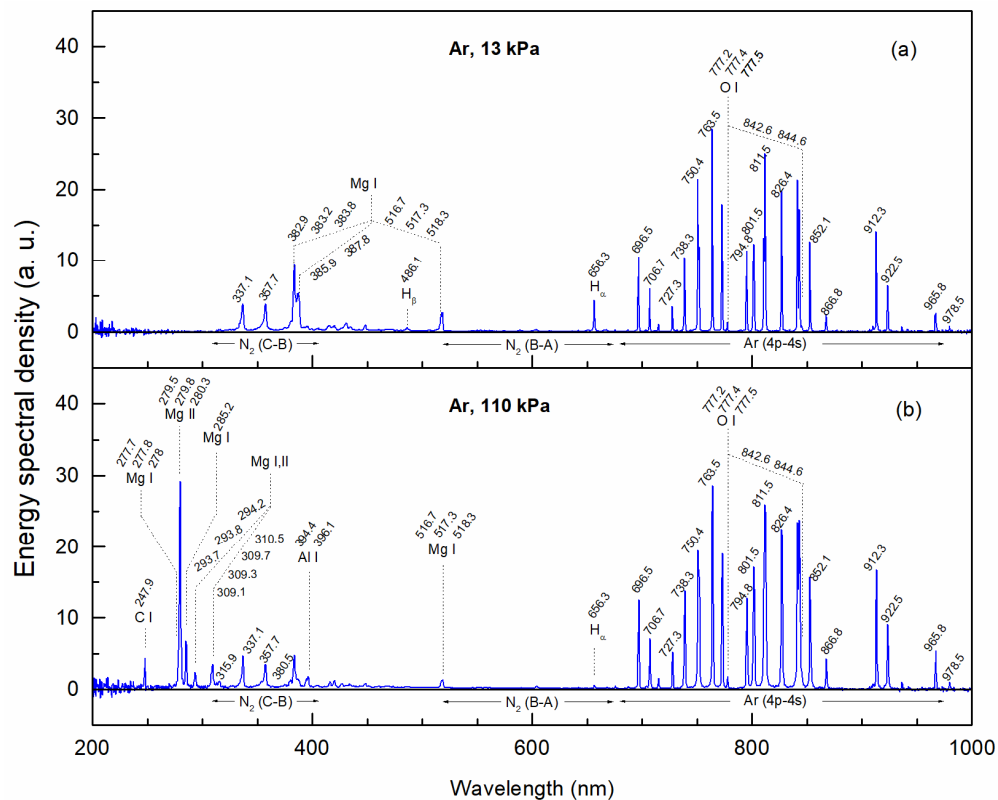


Figure 4. Emission spectra of the nanosecond discharge plasma in argon at a pressure of (a) 13, and (b) 110 kPa.

The second point that is noteworthy is the bands of the second positive system of molecular nitrogen N_2 ($C^3\Pi_u - B^3\Pi_g$) and weakly expressed bands of the first positive system of N_2 ($B^3\Pi_g - A^3\Sigma_u^+$). At the same time, the bands of the first negative system of N_2^+ ($B^2\Sigma_u^+ - X^2\Sigma_g^+$) did not appear in a significant way. The presence of these bands in the emission spectra suggests that there was a small amount of nitrogen admixture in the argon balloon used in the experiment. In addition to the molecular nitrogen bands, there were lines of oxygen atoms O I at 777.2, 777.4, and 777.5 nm as well as at 842.6 and 844.6 nm. It should be noted that the fraction of nitrogen bands and oxygen atoms in the spectral distribution of the energy of the discharge emission remained the same at both low (Figure 4a) and elevated (Figure 4b) pressures, which also indicates the presence of an impurity in the balloon. In addition to the lines of oxygen atoms and bands of molecular nitrogen, the emission spectrum also contained lines of hydrogen H_β (4–2) at 486.1 nm and H_α (3–2) at 656.3 nm, as well as carbon C I at 247.9 nm. Thus, even a small gas admixture could affect the plasma composition. This contamination could be problematic for producing pure metal nanoparticles and powders.

As for the vapors of the electrode material, which were formed during the explosions of microprotrusions on the electrode surface during the flow of a high current through them, their presence was confirmed by the results of the emission spectroscopy. In the emission spectrum, there were many lines of magnesium atoms Mg I (Figure 4) and ions Mg II (Figure 4b, elevated pressure), as well as aluminum atoms Al I (Figure 4b, elevated pressure), from which the high-voltage and grounded electrodes were made, respectively. Particularly strong lines of magnesium ions Mg II were observed at an elevated pressure in the wavelength range of 270–310 nm. This was probably due to the fact that the contact area of the discharge channel was the smallest at a high argon pressure. Therefore, the current density was the highest.

The production of chemical compounds based on the constituent element (Mg) of a cathode or anode is closely related to either the binding energy, formation entropy, or chemical activity of gaseous species preserved in the discharge plasma. The flow of nanoparticles (Figure 1a), visualized in [21], were deposited as a powder layer onto the surface of the grounded electrode and the side wall of the discharge chamber.

The structure of the particles synthesized during the diffuse nanosecond discharge in argon at an elevated pressure (110 kPa) is shown in Figure 5.

The particles exhibited a rectangular shape (Figure 5a,c) and coupled with each other into large (~500 nm) agglomerates. The characteristic deformation TEM contrast was observed to be stronger near the boundaries, which was related to internal elastic stresses or dislocation-type defects. Selected area electron diffraction (SAED) (Figure 5b) revealed the formation of a single phase based on MgO (ICDD # 04-003-7162) with a face-centred cubic lattice (Pearson symbol is cF8). This was confirmed by a nanobeam diffraction analysis performed on the individual particles (inset in Figure 5a). The particle size varied in the range of 10–60 nm. The mean size evaluated by a series of dark-field images (Figure 5d) was 30 ± 8 nm.

At a low pressure of argon (13 kPa), we observed a high-dispersed net of nanoparticles (Figure 6).

The particles tended to roll up into spherical balls of ~200 nm in diameter (Figure 6c). Using a dark-field imaging mode (Figure 6d), we were able to distinguish the separate particles and examine their mean size (13 ± 8 nm). In this case, the standard deviation of the crystallite size was much larger due to the coagulation and sticking of the particles. The corresponding SAED pattern (Figure 6b) exhibited solid and thick rings, confirming a nanocrystalline structure of the powder. The indexing of the SAED and nanobeam diffraction (Figure 6a, inset) patterns showed that the synthesized particles belongs to the tP6 MgF_2 phase with a tetragonal structure (ICDD # 04-005-4303). The shape of the particles was presumably round-like.

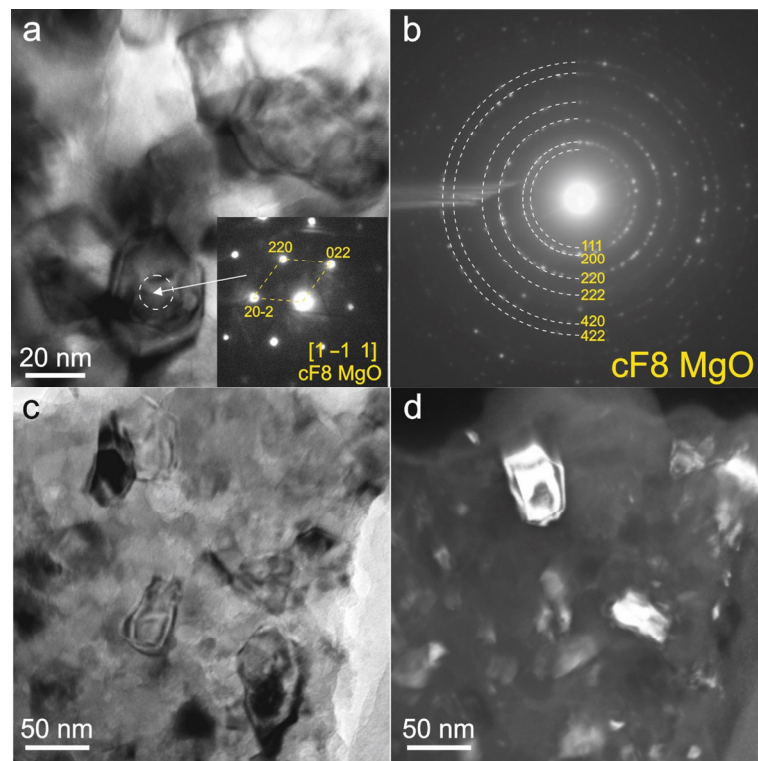


Figure 5. TEM images of the nanoparticles synthesized during the nanosecond discharge in argon at elevated pressure (110 kPa): (a,c) bright-field images, (b) selected area diffraction pattern, and (d) dark-field image. The nanobeam diffraction pattern belonging to the MgO phase is given in the inset.

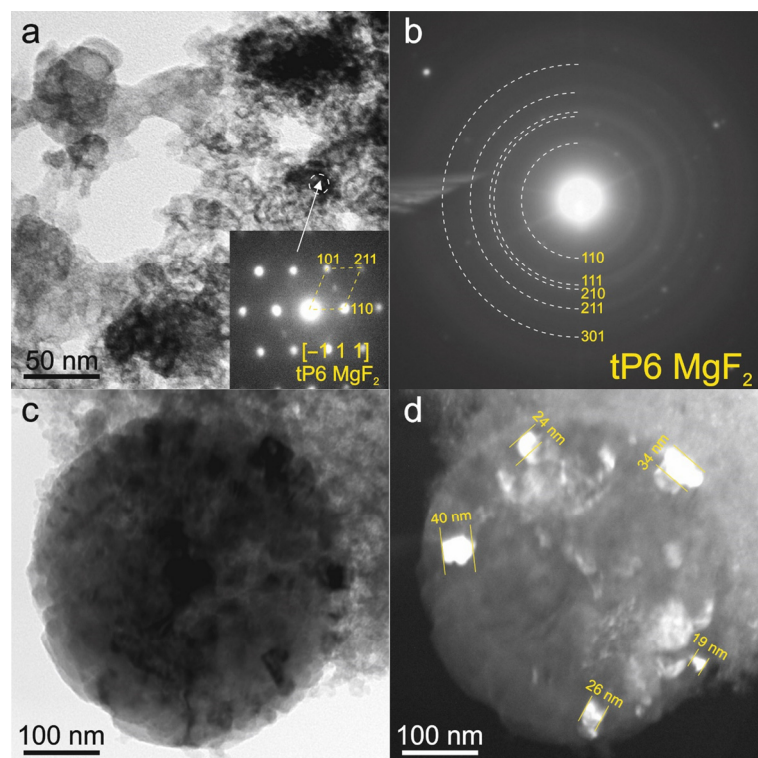


Figure 6. TEM images of the nanoparticles synthesized during the nanosecond discharge in argon at low pressure (13 kPa): (a,c) bright-field images, (b) selected area diffraction pattern, and (d) dark-field image. The nanobeam diffraction pattern belonging to the MgF₂ phase is given in the inset.

It is important to note that among the hundreds of powder particles analyzed in the TEM, we did not find traces of the presence of MgAl_2O_4 or Al_2O_3 , both in the micro and nanobeam diffraction analysis patterns. According to the phase equilibrium diagram of the Mg–Al–O system [22], oxide phases ordered by the type MgO, MgAl_2O_4 , or Al_2O_3 are indeed expected oxidation products. Aluminum–magnesium composite deoxidation may occur via transformation from MgO to $\text{MgO}\cdot\text{Al}_2\text{O}_3$ and Al_2O_3 . The possible phase transitions in the Mg–Al–O system are determined by the activity coefficients of the aluminum, magnesium, and oxygen atoms, as well as their concentrations. The thermodynamic analysis carried out in this work showed that the share of oxygen required for the deoxidation of aluminum is only 3.20 PPM. In turn, the deoxidation limit of magnesium is higher (4.39 ppm). From this, it follows that, because of the high oxygen activity of Al and Mg, we can expect the formation of a two-phase mixture of $\text{MgO} + \text{Al}_2\text{O}_3$ through the reaction of $\text{MgO}\cdot\text{Al}_2\text{O}_3 = 2[\text{Al}] + [\text{Mg}] + 4[\text{O}]$ (if an appropriate content of oxygen is preserved in the reaction zone). According to the optical spectra (Figure 4), numerous high-intensity lines of magnesium and a single line of aluminum were found. Qualitatively, this indicates the predominance of Mg species in the plasma. Based on the type of cathode used and the conditions of the nanosecond discharge plasma in argon, the most likely scenario is the formation of magnesium oxides (MgO) when the oxygen content is up to 20 ppm [22]. The formation of compounds according to the type of MgAl_2O_4 requires a much larger partial pressure of oxygen and higher temperatures; therefore, presumably, we did not find the phase data using TEM.

The quantitative EDS/TEM point analysis was performed in the local areas shown by Arabic numerals in Figure 7.

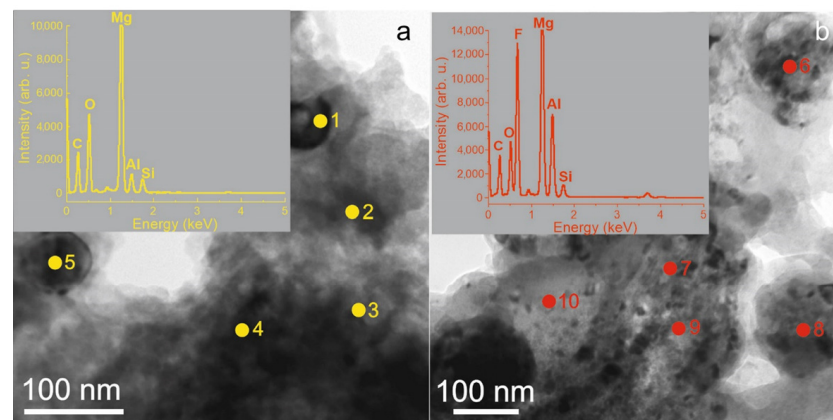


Figure 7. Bright-field TEM images of the powder mixture produced during the nanosecond discharge in argon at (a) elevated (110 kPa), and (b) low (13 kPa) pressures. EDS/TEM analysis was performed from the points (1)–(10) marked in (a,b). Typical EDS spectra are shown in the insets.

The results of the chemical composition evaluation are listed in Table 1.

One can see that the Mg-bearing powder was rich in oxygen (inset in Figure 7a) in the case of the powder obtained at an elevated pressure (110 kPa). At a low pressure (13 kPa), all the particles had a large amount of fluorine (inset in Figure 7b). Based on the TEM (Figures 5 and 6) and EDS data, we may conclude that, due to cathode erosion, the high-energy Mg ions tended to form oxides or fluorides. The mean chemical compositions (Table 1) of the observed Mg-bearing compounds were $\text{Mg}_{40}\text{O}_{53}\text{Al}_4\text{Si}_3$ (at. %) and $\text{Mg}_{27}\text{O}_{22}\text{F}_{41}\text{Al}_8\text{Si}_2$ (at. %). The Al and Si impurities originated from the low purity of the cathode.

The presence of magnesium fluorides at a low argon pressure was an unexpected result. There is no exact clarity on where the fluorine came from. No lines of atoms and ions of fluoride were found in the optical emission spectrum (Figure 4). However, we assume that the fluorine could have appeared as a result of the interaction between the

discharge plasma and the surface of the insulator made of fluoroplastic. The fact is that, with a decrease in gas pressure, the reduced electric field strength increased. For this reason, the discharge could develop not only along the shortest path, but also along the surface of the fluoroplastic insulator: from the high-voltage electrode to the chamber walls (see Figure 1a).

Table 1. Quantitative results of the EDS/TEM analysis performed from the points (Figure 7).

Point Number	Mg (at. %)	Al (at. %)	Si (at. %)	O (at. %)	F (at. %)
$p_{Ar} = 110 \text{ kPa}$					
1	44	4	3	49	–
2	44	3	1	52	–
3	40	3	2	55	–
4	42	3	3	52	–
5	32	7	4	57	–
$p_{Ar} = 13 \text{ kPa}$					
6	32	4	1	13	50
7	21	8	3	33	35
8	24	14	2	21	39
9	26	10	2	19	43
10	29	4	3	24	40

4. Conclusions

The possibility of the production of nanoparticle powders in a diffuse nanosecond discharge at atmospheric pressure and high overvoltages at different pressures, including atmospheric pressure, was studied. The implementation of the nanosecond voltage pulses of a negative polarity across the gap filled with argon, either at low or elevated pressures, resulted in the formation of low-temperature plasma. Metal plasma was produced due to the explosion of microprotrusions on the electrode surface. Nanoparticles were formed during the adiabatic expansion of this metal plasma. Magnesium oxides (MgO) and magnesium fluoride (MgF₂) phases with face-centered cubic and tetragonal lattices were found. It was shown that magnesium oxides were formed during the discharge in argon at an elevated pressure. The magnesium atoms interacted with the oxygen atoms formed during a dissociation of the oxygen molecules that presented in argon as a residual impurity. Thus, the production of pure Mg particles cannot be performed under the proposed experimental conditions. Magnesium fluoride was found in the fabricated powder mixture produced during the diffuse nanosecond discharge in argon at a low pressure. Within the framework of the hypothesis, it was assumed that fluorine molecules could be released from the surface of the fluoroplastic insulator of the discharge chamber due to the fact that, at a low argon pressure, the discharge also occurred on the surface of the insulator, despite the longer path. This will be verified by us as part of a separate experiment in future studies. Since fluorine is a stronger oxidizing agent than oxygen, magnesium fluoride nanoparticles were formed. It can be assumed that the combination of a discharge over the surface of the fluorine-containing materials (fluoroplastic) with a diffuse nanosecond discharge in an inert gas of a high pressure and, at the same time, of a low purity, could serve as a method for harmlessly obtaining fluoride nanopowders of various metals used for the production of nanoceramics.

The problem of the presence of impurities among the magnesium oxide particles could be solved by the use of magnesium alloys with a reduced content of atoms of other elements, as well as the use of pure gases. In addition, a number of constructive changes should be made to avoid the development of discharge along the surface of the insulators.

An increase in the productivity of the method could be achieved by the concentration of the discharge current, as well as an increase in the pulse repetition rate by two, or even three orders. At the same time, it is important to save the plasma cold, as well as to avoid electrode heating.

Author Contributions: Conceptualization, D.B. and D.S.; methodology D.B., D.S., V.S. and K.S.; validation, D.B., D.S., V.S. and K.S.; formal analysis, D.B. and V.S.; investigation, D.B., D.S., V.S. and K.S.; resources, D.S. and V.S.; data curation, D.B.; writing—original draft preparation, D.B. and V.S.; writing—review and editing, D.B., D.S., V.S. and K.S.; visualization, D.B. and V.S.; supervision, K.S. and D.S. All authors have read and agreed to the published version of the manuscript.

Funding: The study was supported by the Russian Science Foundation under grant 22-19-00265, <https://rscf.ru/en/project/22-19-00265/> (accessed on 25 May 2023).

Institutional Review Board Statement: Not applicable.

Informed Consent Statement: Not applicable.

Data Availability Statement: Not applicable.

Conflicts of Interest: The authors declare no conflict of interest.

References

1. Boch, P.; Niepce, J.-C. *Ceramic Materials: Processes, Properties, and Applications*; ISTE: London, UK, 2010.
2. Shekhawat, D.; Singh, A.; Bhardwaj, A.; Patnaik, A. A Short Review on Polymer, Metal and Ceramic Based Implant Materials. *IOP Conf. Ser. Mater. Sci. Eng.* **2021**, *1017*, 12038. [[CrossRef](#)]
3. Fiume, E.; Magnaterra, G.; Rahdar, A.; Verné, E.; Baino, F. Hydroxyapatite for Biomedical Applications: A Short Overview. *Ceramics* **2021**, *4*, 542–563. [[CrossRef](#)]
4. Rödel, J.; Kounga, A.B.N.; Weissenberger-Eibl, M.; Koch, D.; Bierwisch, A.; Rossner, W.; Hoffmann, M.J.; Danzer, R.; Schneider, G. Development of a roadmap for advanced ceramics: 2010–2025. *J. Eur. Ceram. Soc.* **2009**, *29*, 1549–1560. [[CrossRef](#)]
5. Karadimas, G.; Salonitis, K. Ceramic Matrix Composites for Aero Engine Applications—A Review. *Appl. Sci.* **2023**, *13*, 3017. [[CrossRef](#)]
6. Tite, M.S. Ceramic Production, Provenance and Use—A Review. *Archaeometry* **2008**, *50*, 216–231. [[CrossRef](#)]
7. Fang, Y.; Agrawal, D.; Skandan, G.; Jain, M. Fabrication of translucent MgO ceramics using nanopowders. *Mater. Lett.* **2004**, *58*, 551–554. [[CrossRef](#)]
8. Bai, L.; Ouyang, Y.; Yuan, F. Progress in Preparation of ZrB₂ Nanopowders Based on Traditional Solid-State Synthesis. *Nanomaterials* **2021**, *11*, 2345. [[CrossRef](#)] [[PubMed](#)]
9. Hong, Y.; Fan, H.; Li, B.; Guo, B.; Liu, M.; Zhang, X. Fabrication, biological effects, and medical applications of calcium phosphate nanoceramics. *Mater. Sci. Eng. R Rep.* **2010**, *70*, 225–242. [[CrossRef](#)]
10. Najeeb, S.; Khurshid, Z.; Zafar, M.S.; Khan, A.S.; Zohaib, S.; Marti, J.M.N.; Sauro, S.; Matinlinna, J.P.; Rehman, I.U. Modifications in Glass Ionomer Cements: Nano-Sized Fillers and Bioactive Nanoceramics. *Int. J. Mol. Sci.* **2016**, *17*, 1134. [[CrossRef](#)] [[PubMed](#)]
11. Ming, W.; Jiang, Z.; Luo, G.; Xu, Y.; He, W.; Xie, Z.; Shen, D.; Li, L. Progress in Transparent Nano-Ceramics and Their Potential Applications. *Nanomaterials* **2022**, *12*, 1491. [[CrossRef](#)] [[PubMed](#)]
12. Sadykov, V.; Usoltsev, V.; Yermeev, N.; Mezentseva, N.; Pelipenko, V.; Krieger, T.; Belyaev, V.; Sadvovskaya, E.; Muzykantov, V.; Fedorova, Y.; et al. Functional nanoceramics for intermediate temperature solid oxide fuel cells and oxygen separation membranes. *J. Eur. Ceram. Soc.* **2013**, *33*, 2241–2250. [[CrossRef](#)]
13. Pai, D.Z. Nanomaterials synthesis at atmospheric pressure using nanosecond discharges. *J. Phys. D Appl. Phys.* **2011**, *44*, 174024. [[CrossRef](#)]
14. Itatani, K.; Tsujimoto, T.; Kishimoto, A. Thermal and optical properties of transparent magnesium oxide ceramics fabricated by post hot-isostatic pressing. *J. Eur. Ceram. Soc.* **2006**, *26*, 639–645. [[CrossRef](#)]
15. Beloplotov, D.; Tarasenko, V.; Sorokin, D.; Zhang, C.; Shao, T. Positive and negative streamers in air and nitrogen in a sharply inhomogeneous electric field under conditions of runaway electron generation. *High Volt.* **2022**, *8*, 527–537. [[CrossRef](#)]
16. Efanov, V.; Efanov, M.; Komashko, A.; Kriklenko, A.; Yarin, P.; Zazoulin, S. High-Voltage and High-PRF FID Pulse Generators. In *Ultra-Wideband, Short Pulse Electromagnetics 9*; Sabath, F., Giri, D.V., Rachidi-Haeri, F., Kaelin, A., Eds.; Springer: New York, NY, USA, 2010; pp. 301–305. [[CrossRef](#)]
17. NIST Atomic Spectra Database (ver. 5.10). Available online: <https://www.nist.gov/pml/atomic-spectra-database> (accessed on 5 October 2014).
18. Raizer, Y.P. *Gas Discharge Physics*; Springer: Berlin/Heidelberg, Germany, 1991.
19. Tarasenko, V.F. *Runaway Electrons Preionized Diffuse Discharges*; Nova Science Publishers: New York, NY, USA, 2014.
20. Mesyats, G.A. Ectons and their role in plasma processes. *Plasma Phys. Control Fusion.* **2005**, *47*, A109–A151. [[CrossRef](#)]

21. Beloplotov, D.V.; Lomaev, M.I.; Sorokin, D.A.; Tarasenko, V.F. Blue and green jets in laboratory discharges initiated by runaway electrons. *J. Phys. Conf. Ser.* **2015**, *652*, 12012. [[CrossRef](#)]
22. Wang, H.; Yu, P.; Zhou, X.; Wang, Y.; Lv, X. Three-dimensional stability diagram of Al–Mg–O inclusions in molten steel. *J. Mater. Res. Technol.* **2021**, *12*, 43–52. [[CrossRef](#)]

Disclaimer/Publisher’s Note: The statements, opinions and data contained in all publications are solely those of the individual author(s) and contributor(s) and not of MDPI and/or the editor(s). MDPI and/or the editor(s) disclaim responsibility for any injury to people or property resulting from any ideas, methods, instructions or products referred to in the content.